Astron. Astrophys. 319, 282–289 (1997)

ASTRONOMY
AND
ASTROPHYSICS

The radiation belts of Jupiter at 13 and 22 cm

II. The asymmetries and the magnetic field

G.A. Dulk[1,2], Y. Leblanc[1], R.J. Sault[3], H.P. Ladreiter[4], and J.E.P. Connerney[5]

[1] CNRS–URA 264, Departement de Recherche Spatiale, Observatoire de Paris, F-92195 Meudon, France
[2] Department of Astrophysical, Planetary and Atmospheric Sciences, University of Colorado, Boulder, CO 80309, USA
[3] Australia Telescope National Facility, CSIRO, Epping, NSW 2121, Australia
[4] Space Research Institute, University of Graz, Graz, Austria
[5] Planetary Magnetospheres Branch, NASA Goddard Space Flight Center, Greenbelt, MD 20771, USA

Received 11 April 1996 / Accepted 17 June 1996

Abstract. Observations of Jupiter at 13 and 22 cm made with the Australia Telescope in July 1995, reported in Paper I (Leblanc et al. 1996), are interpreted by comparing with models of the magnetic field. The field models used are the O6 and a new, 4th degree and order model due to one of us (JEPC), denoted H4.

1) From our 3-D reconstruction we derive the variation with longitude λ_{III} of the latitude and radial distance of peak radio emissivity: $-10^\circ \lesssim$ lat $\lesssim +13^\circ$, and 1.45 $R_J \lesssim R \lesssim$ 1.75 R_J. These values are in good agreement with the location of the magnetic equator on a surface of constant total field $|B| \approx 1$ G.

2) We present the variation with λ_{III} of the latitude and radial distance of high-latitude peaks in linearly-polarized brightness from a similar 3-D reconstruction. Comparing with calculations from the H4 model, these "mirror points" are in good accord with calculated latitudinal and radial variations for electrons with pitch angle $\alpha_e \approx 27^\circ$ on L shell $L \approx 2.37$ R_J.

3) The variations with λ_{III} (Paper I) of the brightness of regions traversing the east and west limbs (the east-west asymmetry) are compared with field model calculations that take into account the warp of the magnetic equator, i.e. the magnetic declination $D_{\rm mag}$ and the Earth's jovicentric declination D_E that was $D_E = -2.9^\circ$ during our observations. The generally excellent agreement allows us to account for the brightness minimum near $\lambda_{III} \approx 120^\circ$, the maximum near 200°, and the fact that the bright spot near 200° is fainter when crossing the west limb than when crossing the east limb.

4) From the results of (3) we are able to predict the form of the east-west asymmetry when the Earth is at other declinations, up to $D_E = +2.9^\circ$. Some published results substantiate the prediction.

The observations are in better agreement with model H4 than with O6. The discrepancies that remain can be used to improve the field models or further explore the properties of the synchrotron-emitting electrons.

Send offprint requests to: G.A. Dulk

Key words: Jupiter – radio emission – magnetosphere – radiation belts

1. Introduction

In Paper I, Leblanc et al. (1996) present high resolution observations of Jupiter's radiation belts made with the Australia Telescope in July 1995 at 13 and 22 cm. In addition to showing 2-D images that portray the rotational changes in brightness, the paper presents a powerful new visualization, a reconstruction of the belts in 3-D that vividly portrays the warping of the magnetic equator as manifested in the radiation belts around the planet. These data in 2-D and 3-D reveal with unprecedented clarity several puzzling features of Jupiter's radiation belts. The purpose of this paper is to relate these observations to the form of the magnetic field, and thus to obtain further insight into the nature of Jupiter's synchrotron radiation and its magnetic field.

Jupiter's synchrotron emission depends strongly on the strength and geometry of the magnetic field. The field model has been improved (Connerney 1992; 1993), but is not perfect, particularly at small distances, $R \lesssim 2$ R_J that have been poorly sampled by spacecraft. Our observations give us several measurements that we can compare directly with different magnetic field models. We find that we are able to explain most of the observed features, thus the small discrepancies that remain can be used as elements of constraint to improve the magnetic field models and/or to learn more about the synchrotron emitting electron population.

The measurements that are important in this paper are:

1) From our 3-D reconstruction of total intensity we determine the latitude and radial distance of peak emissivity, which lies on the magnetic equator on a surface of constant total field $|B|$, i.e. on a certain L shell.

2) From our 3-D reconstruction of polarized intensity we determine the latitude and radial distance of the high-latitude

peaks in each hemisphere; these lie on a different L shell and reflect the predominant pitch angle of the relativistic electrons.

3) The brightness of the east and west lobes of the radiation belt changes with Jupiter's rotation (e.g. de Pater & Klein 1989; de Pater 1991). When plotted in terms of λ_{III} (the longitude on Jupiter) instead of CML (the longitude facing Earth) some important features become clear that were previously obscure. The brightness curves corresponding to east and west limb passage as a function of longitude have peaks and valleys near the same places, but differ in detail, and the curve of the ratio of east-to-west limb brightness simplifies. (Paper I)

4) In particular, the bright spot of the radiation belts is at $\lambda_{III} \approx 210°$ when viewed on the east limb. It is on the west limb 150° later, not 180° as would be expected. Furthermore, it is brighter when seen on the east limb than on the west limb. (Paper I)

To our knowledge these features have either not been demonstrated previously or have not been explained in a simple, satisfactory way. Our investigation is designed to discover whether they are simply the result of Jupiter's non-dipolar field.

In Sec. 2 we describe the prevailing magnetic field model (O6 model) at 1.5 to 1.7 R_J, the radius of the heart of the radiation belts, and a new, model (H4) developed by one of us (JEPC) that is of 4th degree and order (compared with 3rd degree for O6). In Sec. 3 we present the critical observations, some new and some from Paper I, and confront them with the O6 and H4 models: i) We compare the latitude of peak brightness with the latitude of the magnetic equator of O6 and H4, ii) We compare the distance of the peak intensity with the surface of constant $|B|$ in O6 and H4, and iii) We compare the east-west brightness asymmetry with the magnetic declination in O6 and H4. The last shows how the line of sight from the warped magnetic equatorial surface is directed toward or away from an observer, and as a consequence, why the east-west asymmetry depends on the declination of the Earth (D_E). In particular we explain why we observe the bright spot brighter on east limb passage than on west limb passage. Observations at other D_E reported in the literature are evaluated similarly. In Sec. 4 we present data from the linearly polarized intensity relating to the electron distribution that travels to relatively high latitudes; from the measured latitude and radial distance of the mirror regions we derive the L shell and the pitch angle of these electrons. In Sec. 5 we give a summary of our findings and a discussion of the magnetic field models.

2. The magnetic field models O6 and H4 near 1.5 R_J

In this section we present certain properties of Jupiter's magnetic field that we then will relate to our observations: the latitude, radius and magnetic declination of the magnetic equator at 1.5 to 1.75 R_J.

The commonly-used O6 model of the magnetic field (Connerney 1992; 1993) is of 3rd degree and order, containing dipole, quadrupole and octupole terms. It is based mainly on Pioneer 11 data and to some extent on Voyager 1 data. Among possible solutions it was chosen to agree best with observations of the UV aurora, Io flux tube, and radio emissions.

The H4 model, which will be described in detail elsewhere, is hexadecapole, of 4th degree and order. It also is fitted to magnetometer observations by Pioneer 11 and Voyager 1, but is also tightly constrained to fit the observed footprint of the Io flux tube as observed using the Infrared Telescope Facility on Mauna Kea, Hawaii (Connerney et al. 1993). Essentially no systematic departure of the computed Io L-shell from that determined by observations was allowed. Thus the model is expected to reflect more accurately the geometry of the magnetic field close to the planet. The H4 model is independent of data from observations presented here.

We are particularly concerned with the region of the field near the magnetic equator at 1.4 to 1.7 R_J, where $|B| \approx 1$ G, because the center of the radiation belts lies there. From here onward, the "magnetic equator" is defined as the surface where $|B|$ has a minimum along each field line. A relativistic electron with pitch angle $\alpha_e = 90°$ remains in this magnetic equator and drifts around Jupiter along a path of constant B. Similarly electrons with $\alpha_e \gtrsim 80°$ follow this magnetic equator closely.

Synchrotron radiation from $\gtrsim 10$ MeV electrons is tightly beamed in the direction of the electron's instantaneous motion. Electrons with pitch angles $\gtrsim 80°$, which form one of Jupiter's two relativistic electron populations (see Paper 1), thus produce radiation that is beamed to within about 10° of the perpendicular to the field lines at the magnetic equator. Therefore the maximum of synchrotron radiation is concentrated near the magnetic equator as just defined.

Because of this tight beaming, observations made from Earth depend greatly on where it is located relative to Jupiter's equator. The main parameter is the declination of the Earth as seen from Jupiter, i.e. its distance north or south of Jupiter's rotational equator. Complications arise because of the difference between jovigraphic and jovicentric coordinates. In the astronomical ephemeris, D_E is given in jovigraphic coordinates, whereas jovicentric coordinates are of more relevance when considering the magnetic field. (The JPL ephemeris uses jovicentric coordinates.) As the magnetic field is of paramount importance in this paper, we will use jovicentric coordinates and convert the astronomical ephemeris value of D_E with the relation

$$\text{lat(jovicentric)} = 0.87 \text{ lat(jovigraphic)}.$$

This is a small angle approximation which is valid if $D_E \ll 1$ radian. At the time of our observations in July 1995, the jovigraphic D_E was –3.3°, hence its jovicentric value is $D_E = -2.9°$.

2.1. Magnetic declination and beaming of radiation

When discussing the east-west asymmetry in Sec. 3.3 and 3.4, the concept of magnetic declination, $D_{\rm mag}$, is of major importance, so we introduce it here. Magnetic declination is familiar to us on Earth as being the angle between true north and magnetic north as read from a compass. *More importantly in the*

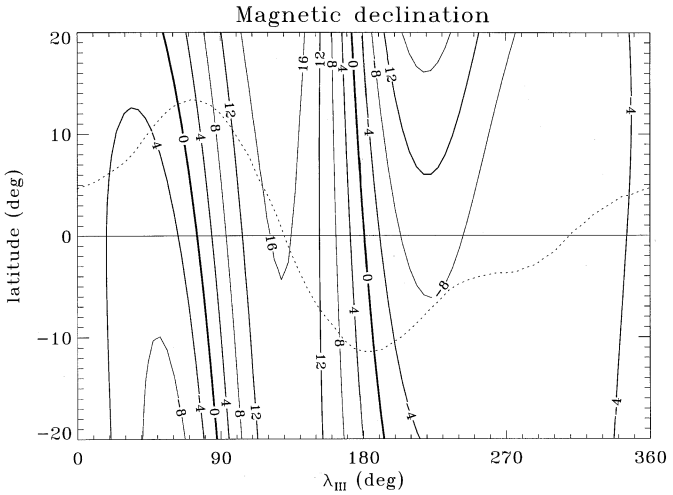

Fig. 1. Contour map from the O6 model of the magnetic declination $D_{\rm mag}$. at 1.5 R_J. The magnetic equator is the dashed line near the jovicentric equator.

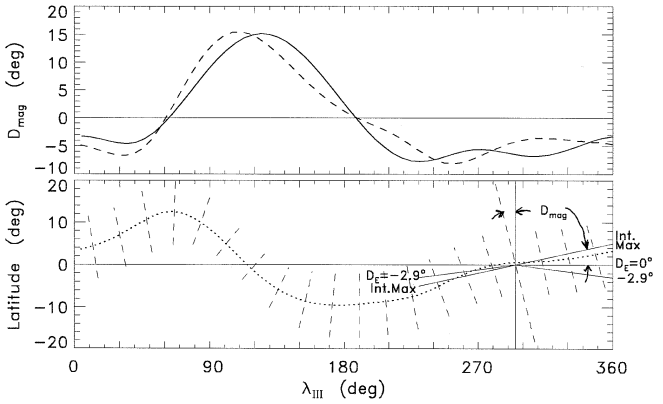

Fig. 2. Top panel: Variation of $D_{\rm mag}$ with longitude for points with $|B| = 1$ G on the magnetic equator; the solid and dashed curves are for the O6 and H4 models respectively. Bottom panel: The dotted line shows the latitude of points with $|B| = 1$ G on the magnetic equator in the H4 model. Several magnetic field lines are shown as dashed lines; the tilt has been exaggerated for clarity. A jovicentric meridian is drawn at $\lambda_{III} = 295°$ and the magnetic declination is indicated there. The lines marked "D_E" ($-2.9°$ in 1995) and "Int. Max" are described further in Fig. 3.

present context, $D_{\rm mag}$ is also the angle between the east-west direction and the perpendicular to the magnetic field lines. As stated above, Jupiter's synchrotron radiation is tightly beamed perpendicular to the field lines and the Earth is always within a few degrees of the east-west direction. Thus $D_{\rm mag}$ plus D_E determine how far the Earth is from the center of the synchrotron beam.

Fig. 1 is a contour map of the magnetic declination $D_{\rm mag}$ at 1.5 R_J on Jupiter as derived from the O6 model of the field (Connerney 1992) using the relation $D_{\rm mag} = \arctan(B_\phi/B_\theta)$, with B_ϕ and B_θ being the azimuthal and colatitudinal components of the field. Superimposed on the contour map is the latitude of the magnetic equator at 1.5 R_J (dashed line). Following the dashed line, we note that $D_{\rm mag} = 0°$ (jovicentric north and magnetic north coincide) at $\lambda_{III} \approx 60°$ and 190°, and the maximum excursions are about +16° and –8° at $\lambda_{III} \approx 120°$ and 230° respectively.

The top panel of Fig. 2 shows in more detail the variation of $D_{\rm mag}$ vs. longitude, here and henceforth for the magnetic equator of $|B| = 1$ G. The solid and dashed curves are for the O6 and H4 models respectively. Most remarkable is the high, relatively narrow peak at $\lambda_{III} \approx 120°$, and the wide, shallow minimum from about 200° to 50°.

While the differences between the curves for the O6 and H4 models are not great, an important one is that the positive excursion in the curve for H4 is much more asymmetric: it has a steeper slope at $\lambda_{III} \approx 60°$, the peak is about 20° earlier, and the slope near 200° is considerably less steep.

The bottom panel, Fig. 2b, is a heuristic presentation of a region near Jupiter's equator, with the dotted line being the magnetic equator. Sample magnetic field lines are shown as dashed with their tilts exaggerated. Consider a typical longitude, $\lambda_{III} = 295°$, where jovicentric north, the solid line, differs from magnetic north, the dashed line.

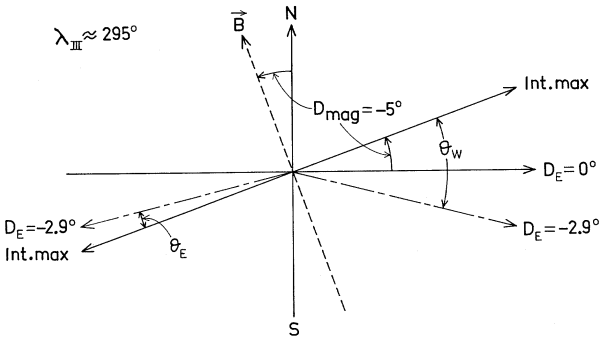

Fig. 3. Enlarged sketch of the region near 295° of Fig. 2b. The rotational equator coincides with $D_E = 0°$, and in 1995 July the Earth was at $D_E = -2.9°$. The magnetic field direction is tilted from north by $D_{\rm mag} = -5°$, and the magnetic equator (the direction of intensity maximum) is tilted from the rotational equator by the same angle. The angles θ_E and θ_W show how far the Earth was from the direction of intensity maximum when this region was observed on the east and west limbs respectively.

Fig. 3 is an enlargement of this region near $\lambda_{III} = 295°$ of Fig. 2b. By definition, $D_E = 0$ coincides with the rotational equator, as shown on the right. Maximum intensity is directed perpendicular to the magnetic field line as shown on the right and left. This direction is at an angle $D_{\rm mag} = -5°$ from the rotational equator (greatly exaggerated for clarity). In 1995 at the time of our observations, $D_E = -2.9°$, as is sketched on the two sides of the figure. *The important point is that, for negative D_E, an observer on Earth lies closer to the direction of maximum intensity when observing from the left-hand side of the diagram, which corresponds to east-limb passage, than when observing from the right-hand side (west limb passage).* That region would be brighter on the east limb (seen there when CML = 295° −

$90° = 205°$) than on the west limb (seen there when CML = $295° + 90° = 25°$).

Returning to Fig. 2b, the tilt of the field lines at 295° longitude corresponds to negative $D_{\rm mag}$ and regions brighter at east limb passage than west limb passage. At longitudes where the field lines are tilted in the opposite direction, positive $D_{\rm mag}$, an observer at negative D_E would see these regions dimmer at east limb passage than at west limb passage. On the top panel of Fig. 2, we see that positive $D_{\rm mag}$ exists only for about 1/3 of a jovian rotation, for λ_{III} between about 65° and 185°.

In order to relate $D_{\rm mag}$ and D_E to the observations, we need the angles between the viewing direction and the direction of maximum intensity for sources on the east limb, θ_E, and on the west limb θ_W. These are given by the relations:

$$\theta_E = |D_{\rm mag} - D_E| \qquad \text{and} \qquad \theta_W = |D_{\rm mag} + D_E| \ ,$$

where in 1995 July, $D_E = -2.9°$. These angles are indicated on Fig. 3. Their maximum value occurs at $\lambda_{III} \approx 130°$ where $D_{\rm mag} = 16°$; then $\theta_E(\max) \approx 19°$ and $\theta_W(\max) \approx 13°$. In the broad minimum between about 200° and 40°, where $D_{\rm mag} \approx -5°$, the corresponding values are $\theta_E \approx 2°$ and $\theta_W \approx 8°$.

3. The observations and the equatorial magnetic field

3.1. Latitude and radial distance of brightness maxima

In Paper I we used the observations over 10 days in July 1995 to make 3-D reconstructions of Jupiter's radiation belts at both 13 and 22 cm, and in both total intensity and linearly polarized radiation. The resultant cubes have resolutions in x, y and z of $0.19 \times 0.19 \times 0.43$ R_J at 13 cm, and $0.31 \times 0.31 \times 0.73$ R_J at 22 cm (the z axis is the spin axis). From the reconstructions we have found the position in 3-D of the peak brightness around Jupiter, its jovicentric latitude and radial distance as a function of longitude λ_{III}. Here we present the data from the 13 cm total intensity observations, but all four 3-D reconstructions (two frequencies, two polarizations) give essentially the same results.

In the top panel of Fig. 4, the symbols give the latitude of peak brightness while the solid and dashed curves show the latitude of the magnetic equator in the O6 and H4 models respectively. The observations and the models are asymmetric in a nearly identical fashion, manifesting the non-dipolar nature of the magnetic field. The observations agree quite well with both models, and from this it is not clear whether they favor the O6 or the H4 model.

The symbols in the bottom panel of Fig. 4 show that the observed excursion in radial distance of peak intensity is about 0.25 R_J, with a wide minimum, 1.45 R_J at $\lambda_{III} \approx 250 - 30°$, and a narrower maximum, 1.7 R_J at $\lambda_{III} \approx 120°$. Here the agreement with the models is reasonable. The general form and the excursion are the same; however, there appear to be real differences. The observations favor the H4 model over the O6 because the peak is more pronounced and occurs at an earlier longitude, and they suggest that a further change in the field model in the same direction would give even better agreement.

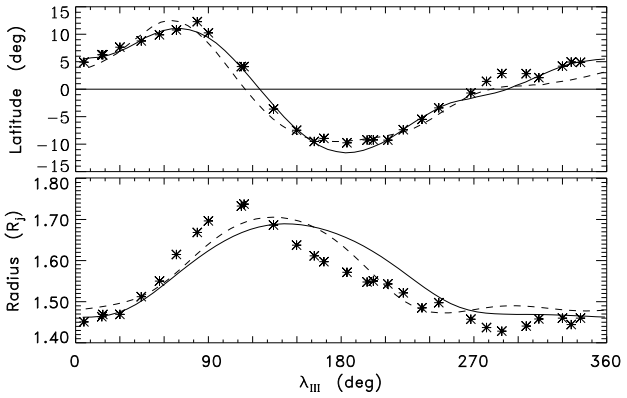

Fig. 4. The symbols show the latitude (upper panel) and radial distance (lower panel) of peak brightness as derived from our 3-D reconstruction of the radiation belts at 13 cm. The solid and dashed curves refer to the points on the magnetic equator where $|B| = 1.023$ G for the the O6 and H4 models respectively.

3.2. Comments on the equatorial brightness maxima

The observations of the previous section reflect the properties of the relativistic electron population that is concentrated at the magnetic equator because the pitch angles are large, 80–90°. The electrons drift around Jupiter in a few days, following the path along the magnetic equator where $B = B_{min} = const \approx$ 1 G, corresponding to L-shell 1.63.

To our knowledge this is the first time that the latitude and radial distance of this path have been directly observed. The latitude variation is in good agreement with the excursion of the magnetic equator near 1.5 R_J in both the H4 and O6 models. The variation of the path in radial distance is from about 1.45 R_J at $\lambda_{III} \approx 270-360°$ to about 1.75 R_J at $\lambda_{III} \approx 120°$, with the latter corresponding approximately to the longitude of the strong magnetic anomaly in the northern hemisphere (the location where the point on the magnetic equator with $|B| = 1.023$ G lies farthest from Jupiter). Our observations suggest that the maximum of this magnetic anomaly is at a longitude 20° smaller than predicted in the H4 model, and 40° smaller than in the O6 model.

As explained in Paper I, our 3-D reconstruction assumes the radiation is isotropic. As this is not the case, the resultant volume emissivity at each point in the 3-D reconstruction is the average emissivity of that point at different rotational phases, e.g. when the point is on the east or west limb or at the center of Jupiter. This assumption has little or no effect on the conclusions just reached about the latitude and radial distance of the maximum intensity of the radiation belt.

The excursion of radial distance derived here is the first from a 3-D reconstruction and the most accurate to date. Previous measurements were always based on 2-D images (e.g. see the review by de Pater & Klein 1989). However, those measurements are not directly comparable with the current results because they can be biased. To see this, consider the profile of synchrotron radiation with radius: the brightness climbs rapidly from near zero at about 1.3 R_J to its maximum at 1.45 to 1.7 R_J,

and then it declines moderately slowly (in Paper I it is detected to 4 R_J). Because of this very asymmetric profile, low resolution images will show the peak intensity to be *outward* from the actual peak. On the other hand, high resolution images show the peaks biased *inward* because the radiation belt is a torus and there is a contribution to the brightness from the portion of the torus at smaller projected radii, closer to the limb. This is the reason that the average radial distance of the maxima in the 2-D image of Paper I was 1.45 R_J, whereas here we find 1.45 to 1.7 R_J. Given these biases, and the fact that the separation varies with Jupiter's rotation, care must be taken in interpreting previous results.

3.3. East-west asymmetry

As described in Paper I, we generated 2-D images at 18 different values of CML, extracting the peak brightness on the east and west limbs (always near the magnetic equator and 1.5 R_J), and converting from CML to λ_{III} by adding 90° to east limb data and subtracting 90° from west limb data.

The symbols in the top and middle panels of Fig. 5 show the peak brightness temperature of the east and west lobes respectively at 22 cm. The brightness on the two limbs has peaks and valleys near the same longitudes, but the variations differ considerably in detail. The brightest region is at $\lambda_{III} \approx 210°$ when crossing the east limb (i.e., when CML$\approx$ 120°). However, when crossing the west limb the brightest region is at a smaller longitude, $\lambda_{III} \approx 180°$ (CML$\approx$ 270°), and is about 100 K fainter. The data at 13 cm are very similar to those at 22 cm (Paper I).

As we have seen in Fig. 3, θ_E and θ_W are measures of the angle between the observer and the perpendicular to the magnetic field at the magnetic equator, with the latter being the direction of maximum emissivity. In Fig. 5 we thus compare the variation of observed brightnesses vs. λ_{III} with the curves of θ_E in the top panel and θ_W in the middle panel derived from the magnetic field models. We are struck by the resemblance. The amplitude and zero level of the ordinate for θ_E are the only free parameters; they were chosen to give a reasonable match to the brightness maximum and minimum of east limb data.

The H4 model (dashed line) gives a distinctly better fit to the data than does the O6 model (dot-dashed line), particularly near the prominent valley at $\lambda_{III} \approx 120°$. The dotted line, from H4 model at 6° intervals, shows peaks that are weak or absent in the heavy dashed line that has 42° resolution.

The third panel of Fig. 5 shows the ratio of brightness, east limb to west limb, for both 22 and 13 cm. The observed variations at the two wavelengths are simple and similar. They show that emission at east limb passage is brighter than at west limb passage for λ_{III} in the range 180° to 40°, while the west limb curve is brighter in the smaller range 40 to 180°. Thus most of the time the east limb is brighter than the west limb, which accounts for the asymmetry in rotation-averaged maps (e.g. Paper I, Fig. 1). The curves show that the ratio derived from the angles θ_E and θ_W has a similarly simple form and is in good agreement with the observed ratio of brightnesses at most longitudes.

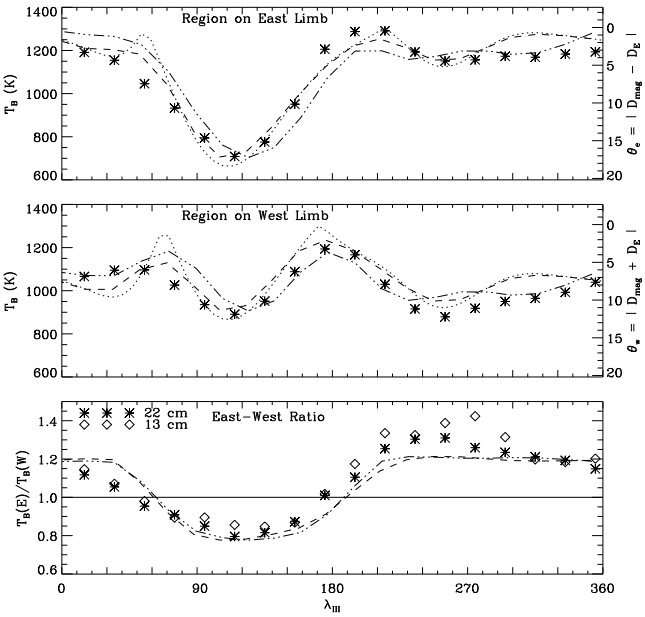

Fig. 5. Variation with λ_{III} of the 22 cm brightness temperature of regions passing the east limb (top panel) and the west limb (middle panel). The symbols show the data. Error bars at 22 cm based on residual fluctuations in the maps are about ±10 K, i.e. smaller than the symbols. Repeatibility using different clean parameters is about 50 K. The H4 model was used to derive θ_E and θ_W, shown by the dotted and dashed lines in the two panels; the ordinate is in degrees as shown on the right. The dotted lines show θ_E and θ_W calculated from the model at 6° intervals, and the dashed lines show them after a running average of width 42° to match the 40° resolution of the observations. The dot-dashed line shows similar, smoothed results from the O6 model. In the bottom panel the east-west ratio is shown by symbols for 22 and 13 cm; the lines show the ratio of the brightnesses corresponding the lines of the upper panel to those of the middle panel.

3.3.1. The east-west asymmetry and the magnetic field

The general agreement in Fig. 5 between the observations and θ_E, θ_W (consequences of D_E and $D_{\rm mag}$ of the H4 model) shows that the warping of the magnetic equatorial surface is the major factor leading to the east-west asymmetry. However, we should be aware that θ_E and θ_W are simply measures of the angle between the observer and the direction of maximum emissivity, and that there is as yet no physical model that relates these angles to the radiation intensity.

With this in mind, there remain some discrepancies between the observations and the predictions of the magnetic field models. One is at $\lambda_{III} \approx 60°$ where a narrow peak is predicted for both east and west limbs by the H4 model (the dotted line representing 6° intervals). This is not seen, partly but not entirely due to our limited resolution in λ_{III}. More substantial is the fact that the data lie below the H4 model prediction from about 270° to 360°. The agreement is better with the O6 model (dot-dashed line) in this range.

Several features of Fig. 5 deserve special mention. The minimum of brightness at $\lambda_{III} \approx 120°$ for both east and west limbs is certainly the consequence of the large warp, $D_{\rm mag} \approx +16°$, at

that longitude. The direction to Earth is far from the direction of intensity maximum, i.e. far from the perpendicular to the field lines at the magnetic equator. For negative D_E, as in 1995, the minimum is deeper for the east limb because $\theta_E \approx 19°$ while θ_W is about 13°. It is only near this longitude of positive $D_{\rm mag}$ (compare with Fig. 2a) that regions passing over the west limb are brighter than when passing over the east limb.

The major maximum of brightness, observed at $\lambda_{III} \approx 180°$ for the west limb and $\lambda_{III} \approx 210°$ for the east limb, are related to the positions where $D_{\rm mag} = \pm 2.9°$. From Fig. 2a we see that the curves for both the H4 and O6 models have a negative slope at these longitudes, reaching +2.9° (maximum brightness on west limb) earlier by 20–30° than it reaches –2.9° (maximum brightness on east limb). By considering only $D_{\rm mag}$ and D_E, we would expect there to be two peaks of nearly equal brightness for both east and west limb passage, at longitudes where $D_{\rm mag} = \pm 2.9°$. In fact, the maximum near 200° is brighter than the one near 60°, with the latter not evident in the data. We cannot account for this difference in terms of $D_{\rm mag}$ in the O6 model where the big peak in Fig. 2a is almost symmetrical. However, in the H4 model the upward slope at $\lambda_{III} \approx 60°$ is much steeper than the downward slope near 200°.

The consequence of this difference is evident in Fig. 2b: near 60° the field line direction changes rapidly so that the observer views the region perpendicular to the field with a small line of sight, leading to a small optical depth and hence low brightness. On the other hand, near 200° the field line direction changes quite slowly and so the corresponding line of sight is relatively large, about 2.8 times larger than near 60°. With the source being optically thin, the extra path length increases the optical depth and hence the brightness. It is this feature of the magnetic field that produces the "bright spot" at $\lambda_{III} \approx 180° - 220°$.

3.4. East-west asymmetry at other D_E

The relationship of the angles θ_E and θ_W with D_E, as given at the end of Sec. 2, shows that when D_E=0, then $\theta_E = \theta_W$, and so the brightness at east and west limb passage is predicted to be the same, irrespective of λ_{III}.

When D_E is positive, e.g. +2.9°, then the brightness curves for east and west limb passage in Fig. 5 are predicted to be reversed from July 1995 when D_E was –2.9°. In particular, in the longitude range 60-190° the brightness at east limb passage should be higher than at west limb passage and the east-west ratio of brightness temperature should be greater than unity only in that longitude range.

In the literature, the east-west asymmetry has been described only by the east-west brightness ratio vs. CML, not λ_{III}, and this contains insufficient information to reconstruct the brightness ratio vs. λ_{III} or the east and west limb brightness variations. However, from the brightness contours in Fig. 6 of de Pater (1980) we are able to estimate these variations for the Westerbork observations of 1977 when $D_E = +2.2°$. We find that the east-west ratio vs. λ_{III} was greater than unity only in the longitude range 80-210°. This is in good agreement with the prediction from the magnetic field model.

Concerning the bright spot, we have shown that when $D_E = -2.9°$, it is located at $\lambda_{III} = 210°$ when seen on the east limb, and at 180° when seen on the west limb. When $D_E = +2.9°$, these longitudes are predicted to reverse. The excursion in longitude of the bright spot on either limb, from $D_E = -2.9°$ to +2.9° should be only about 30°.

4. Mirror regions at higher latitudes

In VLA observations made in total intensity, de Pater and Jaffe (1984) have noted maxima in the emission at a latitude of about ±35°. These have been attributed to a population of electrons with small pitch angles near 2–3 R_J. As shown in Paper I, they are evident in our super-resolved total intensity images at 22 cm, in the 13 cm images, in linearly polarized radiation, and particularly in 3-D reconstructions in which effects of different regions along the line of sight are reduced or eliminated.

From the 3-D reconstruction of the linearly polarized emission, we measured the latitude and radial distance of the peak polarized brightness around Jupiter in both the northern and southern high-latitude maxima; we refer to these positions as the "mirror points". From the H4 model of the magnetic field we calculated representative values of the total field at the mirror points, $|B_{\rm mir}|$, and traced the field lines to the magnetic equator where we determined $|B_{\rm eq}|$. This procedure gave us two values that we henceforth consider as constants: the field at the mirror points, $|B_{\rm mir}| = 1.57$ G, and the field at the magnetic equator, $|B_{\rm eq}| = 0.33$ G.

With the H4 model and these values of $|B_{\rm mir}|$ and $|B_{\rm eq}|$ we calculated the variation with λ_{III} of the latitude and radial distance of the mirror points. Fig. 6 displays the results in a form similar to that of Fig. 4. The observed latitudes vary from about 25° to 40°, similarly in the two hemispheres. The radial distance varies from about 1.45 to 1.8 R_J in the northern hemisphere, but only from about 1.5 to 1.7 R_J in the southern hemisphere; these values are less precise than those for latitude as reflected in the scatter of the data points.

In Fig. 6 there is good agreement between the observations and the predictions of the H4 model in that the general form of the curves is the same. The observed and predicted values of the radial distance are the same to within the errors. However, there are significant deviations between the observed and predicted values of latitude, particularly at $\lambda_{III} \approx 60°$ and 180° in the northern hemisphere and near 200° in the southern hemisphere. At this point we are unable to ascertain any particular reason for the differences between the predicted and observed latitudes.

The average pitch angle $\langle \alpha_e \rangle$ of the electrons producing the polarized brightness maxima at high latitudes can be derived from $|B_{\rm mir}|$, $|B_{\rm eq}|$ and the relation $|B_{\rm eq}| = |B_{\rm mir}| \sin^2 \langle \alpha_e \rangle$. We obtain $\langle \alpha_e \rangle \approx 27°$. The L shell on which these electrons lie is $L \approx 2.37$ R_J. The radial distance of the magnetic equator from Jupiter for $|B_{\rm eq}| = 0.33$ G varies from 2.27 to 2.5 R_J.

It is doubtful whether relativistic electrons with a pitch-angle distribution that varies smoothly, as does the traditional $\sin \alpha_e$ (e.g. Roberts & Komesaroff 1965), are able to produce the high-

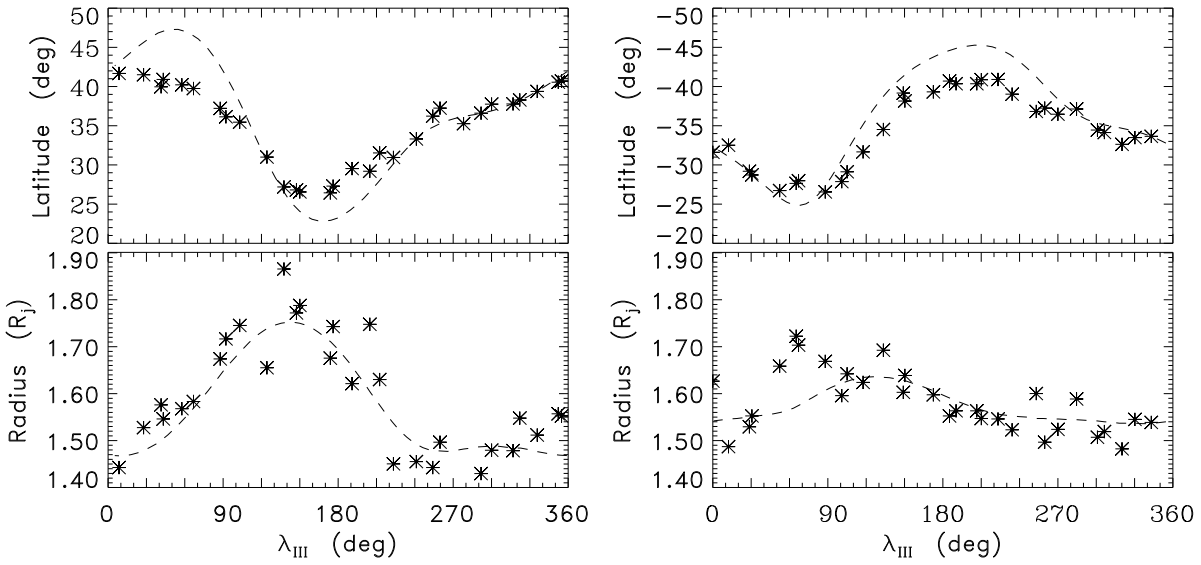

Fig. 6. Plots of the variation with λ_{III} of the latitudes and radii of the high latitude maxima in the 3-D reconstruction of the polarized intensity at 22 cm, the left two panels for Jupiter's northern hemisphere and the right two for the southern hemisphere. The dashed lines are calculated from the H4 model for electrons of 27° pitch angle: $|B_{\rm mir}| = 1.56$ G and $|B_{\rm eq}| = 0.33$ G.

latitude maxima we observe, paricularly at 13 cm and in polarized brightness images, and the high-latitude maxima that de Pater & Jaffe (1984) and de Pater (1991) observed in images from the VLA. A more complicated pitch angle distribution is required, one that has a local maximum near $\alpha_e \approx 27°$. De Pater (1981a, Fig. 3) estimates that electrons with pitch angles $\alpha_e \lesssim 12°$ precipitate into Jupiter's atmosphere, which may account for a cutoff at small α_e. It may be significant that Amalthea's orbit is at 2.5 R_J, the outer edge of the $L = 2.37$ shell; perhaps the high-latitude maxima are related to pitch-angle scattering by disturbances created by Amalthea.

Fischer et al. (1996) report the flux and angular distributions of energetic particles observed by the Galileo probe as it traversed the inner Jovian magnetosphere near the equator. They find that > 8 MeV electrons have an angular distribution with widespread pitch angles at 3.3 R_J, considerably narrower at 1.95 R_J, and narrower yet at 1.85 and 1.55 R_J. These data are consistent with our finding of electrons with small pitch angles and high latitude maxima at $L \approx 2.37$ R_J that are no longer evident inside 2 R_J. However, the Galileo probe data show no evidence of a distinct, second population of electrons in the angular distribution data, probably because the angular resolution is not adequate to see it.

5. Discussion and conclusions

In this study we have presented unique observations, including the first 3-D reconstructions, that show how the multipole character of the Jovian magnetic field is reflected in the synchrotron radio emission. The east-west asymmetry was already known (Branson 1968; Conway & Stannard 1972; de Pater & Jaffe 1984) and extensive calculations including magnetic field models were made by de Pater (1981b). Here we utilize a new approach where the variations in λ_{III} (instead of CML) of the brightness on east and west limb are simply explained by considering the magnetic declination, a parameter that relates to the warping of the magnetic equatorial surface. The bright spot which was first noticed by Branson (1968) is found at λ_{III}= 210° when traversing the east limb, and at λ_{III}= 180° when seen on the west limb. We predict that the excursion in longitude of the bright spot on either limb, should be about 30° when D_E varies from -2.9 to +2.9 °.

From a 3-D reconstruction of the observations we show how the latitude and the peak brightness of the equatorial emission evolve with the rotation of the planet. The derived radial distance varies from 1.45 $R_J \lesssim R \lesssim$ 1.75 R_J, where the maximum excursion corresponds to the magnetic anomaly in the northern hemisphere at λ_{III}= 120°. This is the most accurate measurement to date, because measurements of radial distances of the two maxima in 2-D images contain biases. Since this radial distance of the peak brightness traces out the locus of constant total field on the magnetic equator, our measurements are very sensitive to differences in models of the Jovian magnetic field. Here we have used them to compare the new, 4th degree model H4 with the familiar O6 model; we find better agreement with the H4 model.

The emission due to the low pitch angle population of electrons is clearly seen in the linearly polarized emission in the mirror regions at high latitudes. From the 3-D reconstruction, we measured the latitude and radial distance of the peak brightness in the two hemispheres. As expected, the values differ greatly between the northern and the southern hemispheres. Comparison with the magnetic field model allowed us to determine the L-shell and the average pitch angle of the electrons producing the high-latitude emission.

A complete description of the synchrotron radiation involves a number of parameters that we have little discussed, e.g. the energy distribution of the electrons, their pitch angle distribu-

tion, gradient drift, and radial diffusion (see de Pater 1981a,b). However, our results show that the magnetic field is the main parameter needed to explain the major features of the observations and their complexity. In addition, high resolution observations made at different values of D_E can be used to constrain the magnetic field models.

Acknowledgements. The Australia Telescope Compact Array is part of the Australia Telescope National Facility, CSIRO. We thank T. Oosterloo and R.E. Gooch with help in visualizing the three-dimensional cubes. RJS and YL acknowledge grants from the Australia-France Cooperative Program.

References

Branson N.J.B.A., 1968 MNRAS, 139, 162
Conway R.G., Stannard D., 1972, Nature Phys. Sci. 239, 142
Connerney J.E.P., 1992, In: H.O. Rucker, S.J. Bauer eds., Planetary Radio Emissions III, Austrian Academy of Sciences, p. 13
Connerney J.E.P., 1993, J. Geophys. Res., 98, 18659
Connerney J.E.P., Baron R., Satoh T., Owen T., 1993, Science, 262, 1035
de Pater I., 1980, A&A, 88, 175
de Pater I., 1981a, J. Geophys. Res., 86, 3397
de Pater I., 1981b, J. Geophys. Res., 86, 3423
de Pater I., Jaffe W.J., 1984, ApJS, 54, 405
de Pater I. Klein M.J., 1989, In: M.J.S. Belton, R.A. West, J. Rahe eds., Time Variable Phenomena in the Jovian System, NASA SP-494, p. 139
de Pater, I., 1991, Astron. J., 102, 795
Fischer, H.M., Pehlke, E., Wibberenz, G., Lanzerotti, L.J., Mihalov, J.D., 1996, Science, 272, 856
Leblanc Y., Dulk G.A., Sault R.J., Hunstead R.W., 1996, A&A, this issue (Paper I)
Roberts J.A., Komesaroff M.M., 1965, Icarus, 4, 127

This article was processed by the author using Springer-Verlag TEX A&A macro package version 4.